Journal of Hazardous Materials 110 (2004) 1–12

Journal of Hazardous Materials

www.elsevier.com/locate/jhazmat

# Two-dimensional DNAPL migration affected by groundwater flow in unconfined aquifer

Masashi Kamon [a], Kazuto Endo [b,*,1], Junichi Kawabata [c], Toru Inui [a], Takeshi Katsumi [a]

[a] *Graduate School of Global Environmental Studies, Kyoto University, Sakyo-ku, Kyoto 606-8501, Japan*
[b] *Research Center for Material Cycles and Waste Management, National Institute for Environmental Studies, 16-2 Onogawa, Tsukuba-shi, Ibaraki 305-8506, Japan*
[c] *Kajima Technical Research Institute, Chofu-shi, Tokyo 182-0036, Japan*

Available online 27 April 2004

**Abstract**

The dense non-aqueous phase liquid (DNAPL) migration process was experimentally investigated in a laboratory-scale tank (150 cm width, 82.5 cm height, and 15 cm depth) to assess a site characterization on DNAPL contamination below a groundwater table. The heterogeneous ground of the tank model consisted of Toyoura sand (hydraulic conductivity, $k = 1.5 \times 10^{-2}$ cm/s for void ratio, $e = 0.62$) and silica #7 sand ($k = 2.3 \times 10^{-3}$ cm/s for $e = 0.72$). A series of experiments was carried out with or without lateral groundwater flow. Hydrofluoroether was used as a representative DNAPL. The main results obtained in this study are as follows: (1) the DNAPL plume does not invade into the less permeable soil layer with higher displacement pressure head; (2) the DNAPL plume migrates faster with lateral groundwater flow than without it; (3) lateral groundwater flow does not affect lateral DNAPL migration; rather, it promotes downward migration; and (4) pore DNAPL pressure without groundwater flow is higher than that with it. The above experimental results were compared with numerical analysis. The fundamental behaviors of DNAPL source migration observed experimentally are expected to be useful for assessing the characteristics of two-dimensional DNAPL migration in an aquifer.


*Keywords:* DNAPL migration; Two-dimensional tank test; Groundwater contamination; Pore pressure head

## 1. Introduction

Dense non-aqueous phase liquid (DNAPL), examples of which include trichloroethylene (TCE), tetrachloroethylene (PCE), 1,1-dichloroethylene (DCE,1,1), fluorene, and phenanthrene, whereas examples of light non-aqueous phase liquids (LNAPLs) include BTEX (benzene, toluene, ethylene, and xylene), *n*-hexane, and *n*-pentane. TCE and PCE, known to be major causes of soil and groundwater contamination, are representative substances of DNAPLs. A DNAPL that passes through soil pores may be retained in the pore space as a blob due to the influence of snap-off and by-passing [1]. In such a case, the DNAPL is referred to as residual/irreducible DNAPL. On the other hand, under an immobile condition of DNAPL, if the degree of DNAPL saturation in soil is higher than the residual DNAPL saturation, the DNAPL plume is called a DNAPL pool [2]. Both the residual/irreducible DNAPL and the DNAPL pool have become new source points of soil and groundwater contamination. Subsequently, small amounts of dissolved DNAPL gradually diffuse into groundwater from the source point. As the environmental standard is prescribed by the concentration of solute that dissolved from DNAPL, advection–dispersion methods have mainly been used to simulate dissolved DNAPL contamination [3,4], and permeable reactive barriers (PRBs) have been installed at a contaminated site as a means of passive remediation, thereby preventing the migration of dissolved DNAPL from the site [5,6]. DNAPL, however, exists as a pure liquid at the source of solute contamination (e.g., the current problem of groundwater contamination). Therefore, an evaluation of the mechanism for DNAPL migration is important.

There are only a few reports of NAPL source migration in comparison with those of solute transport. Among the NAPL-related reports, more experimental investigations

* Corresponding author. Tel.: +81-29-850-2228; fax: +81-29-850-2694.
*E-mail address:* k-endo@nies.go.jp (K. Endo).
[1] Formerly, Department of Civil Engineering, Kyoto University.

0304-3894/$ – see front matter © 2004 Elsevier B.V. All rights reserved.
doi:10.1016/j.jhazmat.2004.02.033

**Nomenclature**

| | |
|---|---|
| $h_{cij}$ | capillary pressure head between phases pair of $i$ and $j$ (cm $H_2O$) |
| $h_{dij}$ | displacement pressure head from $j$-phase to another $i$-phase (cm $H_2O$) |
| $h_l$ | pressure head of $l$-phase (cm $H_2O$) |
| $k$ | hydraulic conductivity of water-phase (cm/s) |
| $m$ | van Genuchten (VG) fitting parameter |
| $N$ | van Genuchten (VG) fitting parameter |
| $S_{le}$ | effective $l$-phase saturation |
| $S_{lr}$ | residual/irreducible $l$-phase saturation |
| $S_l$ | degree of $l$-phase saturation |
| $U_C$ | uniformity coefficient of sample |
| $\Delta h_N$ | pressure difference between initial and measured pore DNAPL pressures (cm $H_2O$) |
| $\alpha_{ij}$ | van Genuchten (VG) fitting parameter in $i$–$j$ two-phase system ($cm^{-1}$) |
| $\beta_{ij}$ | scaling coefficient between phases pair $i$ and $j$ |
| $\lambda$ | Brooks & Corey (BC) fitting parameter |
| $\mu_{rl}$ | relative viscosity of $l$-phase (Pa s) |
| $\rho_{rl}$ | relative liquid density ($\rho_l/\rho^*$) |
| $\sigma_{ij}$ | interfacial/surface tension between phases pair of $i$ and $j$ (N/m) |

*Subscripts*

| | |
|---|---|
| A | air phase |
| e | effective |
| N | NAPL phase |
| r | residual/irreducible or relative |
| W | water phase |

have been carried out on LNAPL migration [7–12] than on DNAPL migration. Although experimental studies of DNAPLs are few, some research has been conducted in the 1990s. One-dimensional column tests for the measurement of DNAPL migration characteristics [13,14], two-dimensional tank tests for measuring NAPL migration in a heterogeneous ground system [15,16], tank modeling tests for DNAPL remediation by using a surfactant or a co-solvent [17–19], and the entrapment mechanism of DNAPL in porous media [20,21] were reported for the site characterization and remediation of DNAPL contamination sites. The concept of passive remediation is receiving much attention, because complete remediation to reach an environmental standard is considered to be uneconomical and technically difficult [22,23]. Site characterization, which is the most important concept in passive remediation, requires migration characteristics, extant quantity, and distribution of DNAPLs as indispensable investigation parameters.

In this study, the migration of DNAPL source in an unconfined aquifer was experimentally investigated using a two-dimensional laboratory-scale tank that has a stratified quasi-aquitard with a crack. Tank modeling tests were performed by visual observation and quantitative measurement of pore DNAPL pressure with a new type of probe proposed by Kamon et al. [13], and the experimental results were compared with numerical analysis.

## 2. Experimental setup

### 2.1. Material properties

Toyoura sand and silica #7 sand were used as the aquifer and a quasi-aquitard materials, respectively, for the tank modeling study. These sands have low uniformity coefficients, $U_C$, as shown in Fig. 1. Their physical properties are summarized in Table 1. The hydraulic conductivities, $k$, of Toyoura sand with a dry density of 1.63 g/cm$^3$ ($e = 0.62$) and silica #7 sand with a dry density of 1.53 g/cm$^3$ ($e = 0.72$) are $1.45 \times 10^{-2}$ and $2.33 \times 10^{-3}$ cm/s, respectively.

In immiscible, two-phase flow in porous media, one significant property of a material is saturation-pressure relation, which is described by the degree of water saturation and the capillary pressure head. The relation is usually referred to as an $S$–$p$ (saturation-pressure) relation, water retention curve, or water characteristic curve. The $S$–$p$ relation expresses the specific property of porous media having various pore sizes and particle sizes, and usually depicts an S shape. Capillary pressure head is defined as pressure difference between wet-

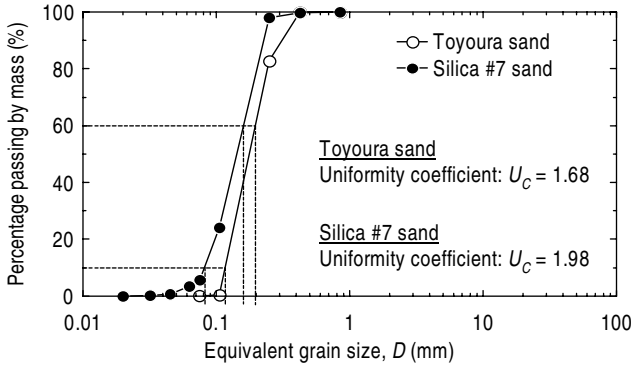


Fig. 1. Grain-size distribution curves.

Table 1
Physical properties of sand samples

| Property | Toyoura sand | Silica #7 sand |
|---|---|---|
| Soil particle density $\rho_s$ (g/cm$^3$) | 2.641 | 2.626 |
| Maximum void ratio $e_{max}$ | 0.97 | 1.21 |
| Minimum void ratio $e_{min}$ | 0.62 | 0.71 |
| Uniformity coefficient $U_C$ | 1.68 | 1.98 |
| Hydraulic conductivity $k$ (cm/s) | $1.45 \times 10^{-2}$ | $2.33 \times 10^{-3}$ |

*Note*: hydraulic conductivities of Toyoura sand and silica #7 sand were measured at void ratios $e = 0.62$ and 0.72, respectively.

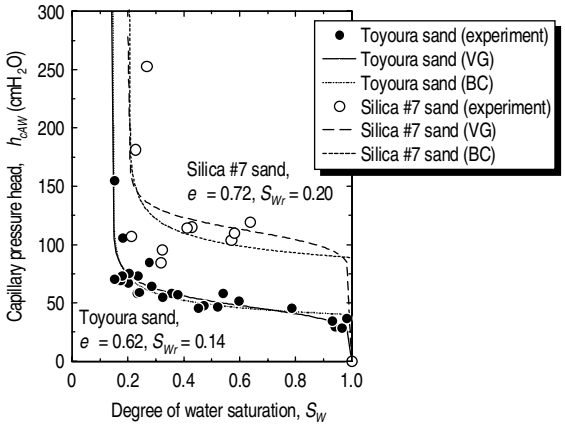


Fig. 2. Saturation-pressure relations ($S$–$p$ relations).

ting (water, in this study) and non-wetting (DNAPL) phases, and is expressed as

$$h_{cNW} = h_N - h_W, \tag{1}$$

where $h_{cNW}$ is the capillary pressure head between DNAPL and water phases, and $h_N$ and $h_W$ are the pore DNAPL pressure head and the water pressure head, respectively. In the case of an air–water two-phase system, the capillary pressure head between air and water phases $h_{cAW}$ can be expressed as $h_{cNW} = h_A - h_W$, where $h_A$ is the pore air pressure head.

The $S$–$p$ relations of the sand samples in a water–air two-phase flow system are illustrated in Fig. 2. The experimental data were fitted by two empirical equations formulated by van Genuchten [24] and Brooks & Corey [25], as shown in Fig. 2. The fitting equation by van Genuchten (VG) is given as:

$$h_{cAW} = \frac{1}{\alpha_{AW}}(S_{We}^{-1/m} - 1)^{1/n} \quad \text{for } h_{cAW} > 0, \tag{2}$$

where $\alpha_{AW}$ and $n$ are the VG parameters, and $m = 1 - 1/n$ [26]. The effective saturation of the water phase, $S_{We}$, is defined by $S_{We} = (S_W - S_{Wr})/(1 - S_{Wr})$, with $S_{Wr}$ being the residual or the irreducible water saturation. The fitting equation by Brooks & Corey (BC) is written as

$$h_{cAW} = h_{dAW} S_{We}^{-1/\lambda} \qquad \text{for } h_{cAW} > h_{dAW}, \tag{3}$$

where $\lambda$ is the pore distribution index and $h_{dAW}$ the displacement pressure head of the reference two-phase system, namely, the displacement pressure head from water phase to another air phase in an initially water-saturated porous medium. The fitting parameters for these models are summarized in Table 2.

Hydrofluoroether (HFE-7100, produced by 3M$^{TM}$) was used as the representative DNAPL. HFE was dyed blue for visual observation. As shown in Table 3, HFE has similar density and viscosity to TCE. The interfacial tension of HFE was measured by means of a standard method used in chemistry, namely, the Ring method [27]. The scaling coefficient $\beta_{NW}$ is generally defined by [29]

$$\beta_{NW} = \frac{\sigma_{AW}}{\sigma_{NW}}, \tag{4}$$

where $\sigma_{AW}$ is the surface tension between water and air phases, and $\sigma_{NW}$ is the interfacial tension between water and DNAPL phases. The scaling coefficient is dependent only on the interfacial tension representing fluid property, and is independent of any soil property. The scaling coefficient is usually used for predicting the $S$–$p$ relation in a water–DNAPL two-phase flow system from that in a water–air system [30]. The scaled VG model in a water–DNAPL system, which is predicted from the $S$–$p$ relation in a water–air system, can be expressed as

$$h_{NW}\beta_{NW} = \frac{1}{\alpha_{AW}}\left(S_{We}^{-1/m} - 1\right)^{1/n} S_{We} = \left[1 + (\alpha_{NW} h_{cNW})^n\right]^{-m} \tag{5}$$

where $\sigma_{NW}$ is $\beta_{NW} h_{dNW}$. By applying the same scaling law to the BC model,

$$h_{cNW}\beta_{NW} = h_{dAW} S_{We}^{-1/\lambda} \qquad \text{or } S_{We} = \left(\frac{h_{dNW}}{h_{cNW}}\right)^{\lambda} \tag{6}$$

is obtained, where $h_{dAW}$ is $\beta_{NW} h_{dNW}$. When the displacement pressure head from the water phase to the air phase

Table 2
Fitting parameters for VG and BC models

| Parameter | Toyoura sand | Silica #7 sand |
|---|---|---|
| VG model | | |
| $S_{Wr}$ | 0.14 | 0.20 |
| $\alpha_{AW}$ (cm$^{-1}$) | 0.0212 | 0.0102 |
| $n$ | 6.57 | 5.7 |
| BC model | | |
| $h_{dAW}$ (cm) | 40.48 | 74.18 |
| $\lambda$ | 4.46 | 3.16 |

Table 3
Properties of HFE-7100 and representative DNAPLs (20 °C)

| Property | HFE-7100 | TCE | PCE | Water |
|---|---|---|---|---|
| Chemical formula | $C_4F_9OCH_3$ | $C_2HCl3$ | $C_2Cl_4$ | $H_2O$ |
| Relative density $\rho_{rl}$ | 1.52 | 1.464 | 1.623 | 1.000 |
| Relative viscosity $\mu_{rl}$ | 0.58 | 0.59 | 0.90 | 1.00 |
| Surface tension $\sigma_{Al}$ (mN/m) | 13.6 | 29.30 | 31.30 | 72.75 |
| Interfacial tension $\sigma_{NW}$ (mN/m) | 35.59[a] | 34.50[b] | 44.40[b] | None |
| Scaling coefficient[c] ($\beta_{NW}$) | 2.044 | 2.109 | 1.639 | 1.000 |
| Vapor pressure (kPa) | 28 | 7.73 | 2.13 | 2.34 |
| Solubility in water (mg/L) | 12 | 1100 | 150 | None |

*Note*: $l$ =W (water) or N (DNAPL).
[a] Measured by Ring method [27].
[b] Reported by Katyal et al. [28].
[c] Introduced by Lenhard and Parker [29].

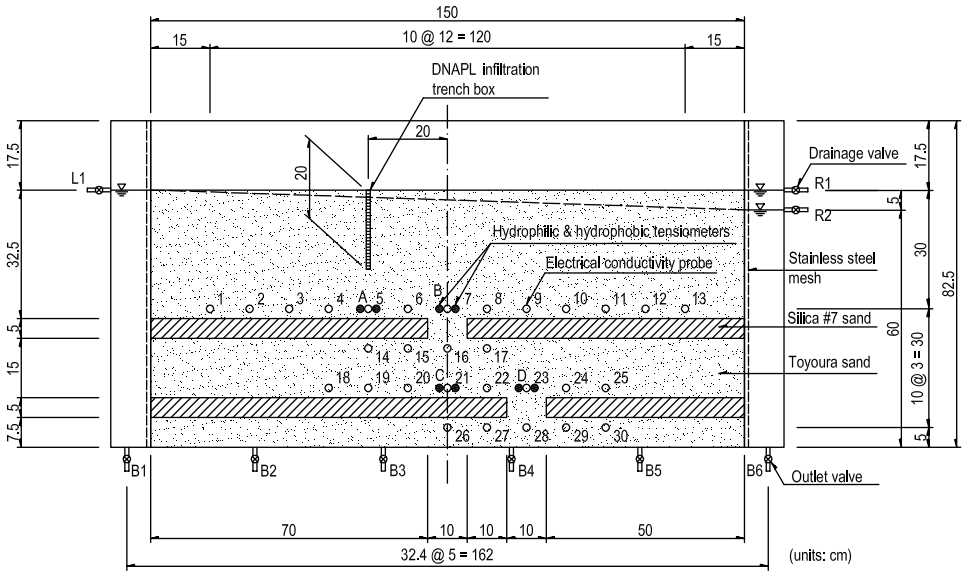


Fig. 3. Schematic diagram of intermediate-scale tank for DNAPL migration tests. Solid circles represent hydrophilic and hydrophobic tensiometers and open circles are electrical conductivity probes.

in a water-saturated porous medium is $h_{dAW}$, the displacement pressure head $h_{dNW}$ from water to DNAPL phases in the same medium can be calculated from $h_{dAW}/\beta_{NW}$.

### 2.2. Tank profiles

A schematic diagram of the laboratory-scale tank used for DNAPL migration tests is illustrated in Fig. 3. The tank had a width of 150 cm, a height of 82.5 cm, and a depth of 15 cm. The tank consisted of a main porous body that was filled with the sands and two chambers located at both sides of the main porous body. The chambers were connected with the main porous body through stainless steel mesh that prevented movement of sands, and allowed for pore liquid drainage. The tank had nine valves for controlling water level, as shown in Fig. 3; three (L1, R1, and R2) were installed on either side of the tank and six (B1, B2, B3, B4, B5, and B6) were installed at the bottom of the tank. The front side of the tank consisted of bulletproof glass for dyed DNAPL migration visualization, and the back side of the tank was made of stainless steel with holes for installing probes. Thirty electrical conductivity probes with three gilded electrodes and four hydrophilic and four hydrophobic tensiometers [13] were installed at the back of the tank before introducing the sands. A new type of electrical conductivity probe was used to measure the degree of water saturation in sandy porous materials, and the hydrophilic and hydrophobic tensiometers were used to measure pore water and DNAPL pressure heads, respectively. However, the data obtained from the electrical conductivity probe are not reported in this paper because the data included noise and thus could not be analyzed.

A 0.05 mol/L sodium chloride solution (0.05 M NaCl) was used as the initial pore liquid in order to increase the reactivity of the electrical conductivity probe. Initially, the inner space of the tank was filled with the NaCl solution, and then the sands were placed by compaction to a height 65 cm by an underwater filling method with vibration. The underwater filling method was deemed successful because the sand did not segregate during sedimentation probably due to the small uniformity coefficient. Quasi-aquitards of 5 cm thickness were located at heights of 7.5 and 27.5 cm from the tank bottom. A trench box of 1 cm width, 20 cm height, and 15 cm depth was used for infiltrating DNAPL into the sand medium without preferential flow in the depth direction. The height of the trench box was set at 20 cm in order to prevent boiling of DNAPL from the bottom of the trench box to the sand surface. To evaluate the influence of lateral groundwater flow on DNAPL migration in an unconfined aquifer, a series of tank modeling tests were conducted without or with lateral groundwater flow. In modeling without groundwater flow, valves L1 and R1 were left open to maintain a hydraulic gradient condition of $i = 0.000$. In the model with lateral groundwater flow at a hydraulic gradient of $i = 5/150 = 0.033$ (corresponding to an average Darcy velocity of 41 cm/day), valves L1 and R2 were left open and the NaCl solution was continuously to be provided from the left-hand side chamber.

## 3. Experimental results

Visual observation results of two-dimensional HFE migration tests without lateral groundwater flow are shown in Fig. 4. Fig. 4a–c show photographs taken 1, 4, and 7 h after HFE infiltration, respectively. The HFE spread bilaterally from the spillage point at the bottom of the trench box, as shown in Fig. 4a. HFE distribution was shaped like a

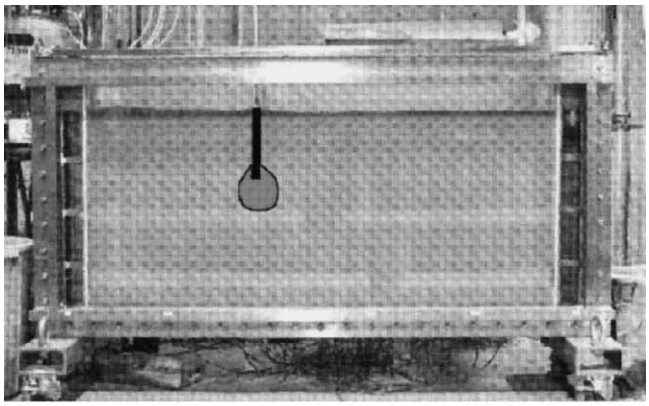

(a)

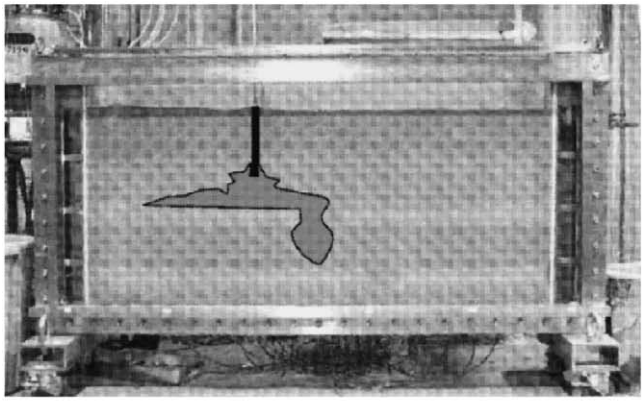

(b)

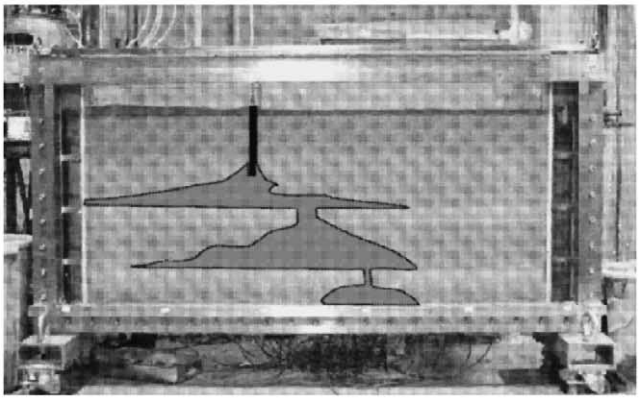

(c)

Fig. 4. HFE migration results without lateral groundwater flow, $i = 0.000$: (a) 1 h after; (b) 4 h after; and (c) 7 h after. To facilitate visualization, HFE-colored regions were retouched by hand tracing. The vertical thick line represents the trench box that penetrated the sandy tank medium, that is, the bottom of the thick line is the spillage point of HFE.

drop of water that comes from a syringe and continues to spread as if a balloon is being inflated. Although the HFE has higher density than water, lateral spreading of HFE from the spillage point was also observed. The tendency of the lateral spreading is consistent with the results obtained using high-viscosity DNAPL by Abu-Hassanein et al. [31]. After reaching the top or surface of the upper quasi-aquitard as shown in Fig. 4b, downward migration of the HFE ceased. However, the HFE continued to migrate laterally along the top of the upper quasi-aquitard until it reached and penetrated the crack. In Fig. 4c, the HFE that reached the lower quasi-aquitard continued to migrate laterally in a manner similar to (b), penetrated the crack, and finally reached the bottom of the tank. It is interesting to note that the HFE eventually reached the right, upper quasi-aquitard and passed through the crack, although the density of HFE is higher than that of water. The same migration was also observed at the lower quasi-aquitard.

Considering actual subsurface conditions, an aquifer without lateral groundwater flow is unrealistic. Therefore, an HFE migration test with lateral groundwater flow was conducted to simulate an aquifer with lateral groundwater flow. Visual observation results of the tank test with groundwater (hydraulic gradient, $i = 5/150 = 0.033$) are shown in Fig. 5. Fig. 5a–c show photographs taken 1, 4, and 7 h after HFE infiltration, respectively. The lateral groundwater flow was controlled by a constant head difference at both ends of the tank and pore water was introduced from left to right.

As shown in Fig. 5a, the HFE spread almost bilaterally from the spillage point and more widely than for the case without groundwater flow. Upward migration of HFE, namely, the boiling of HFE, was observed along the trench box, but this boiling stopped at the level 7 cm above the spillage point (i.e., bottom of the trench box). The HFE that reached the upper quasi-aquitard migrated laterally, similar to the case without groundwater flow. However, the HFE migrated downward at a faster pace for the case with lateral groundwater flow relative to the case without groundwater flow. For example, as shown in Fig. 5b, the HFE reached the bottom of the tank at 4 hours. As groundwater flowed from left to right, rightward migration of the HFE was also expected. However, the HFE showed preferential downward migration. In addition, the HFE migration to the right-hand side of the crack of the upper quasi-aquitard was not observed. In conclusion, lateral groundwater flow with a hydraulic gradient of 0.033 does not affect lateral HFE migration; rather it promotes downward migration.

In both experiments, no HFE infiltration into the quasi-aquitard (silica #7 sand in this study) was observed despite there being only a one order-of-magnitude difference in hydraulic conductivity between the silt and the Toyoura sand layers. This lack of penetration into the quasi-aquitard probably is due to the relatively high displacement pressure head $h_{dNW} = h_{dAW}/\beta_{NW}$ from water to HFE of the silica #7 sand of 36.3 cm $H_2O$ , as calculated by Eq. (6). The infiltration of an immiscible phase into porous media saturated with another immiscible phase, such as the infiltration of DNAPL into an aquitard, depends on the displacement pressure head in the BC model (or a in the VG model) and not the hydraulic conductivity. The displacement pressure head of 36.3 cm $H_2O$ signifies that the pressure is equivalent to that of an approximately 24-cm-high HFE cylinder with a density of 1.52 g/cm$^3$. Consequently, if HFE

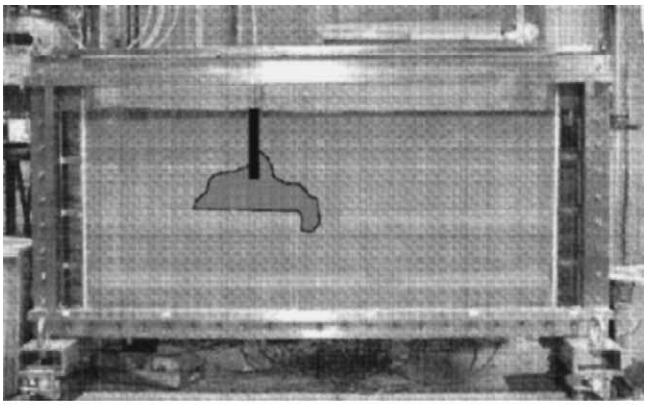

(a)

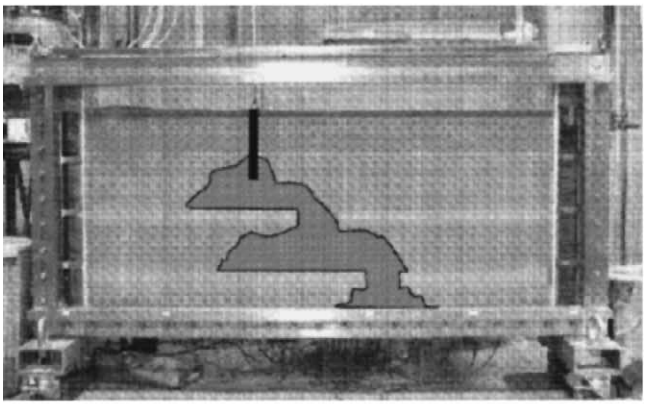

(b)

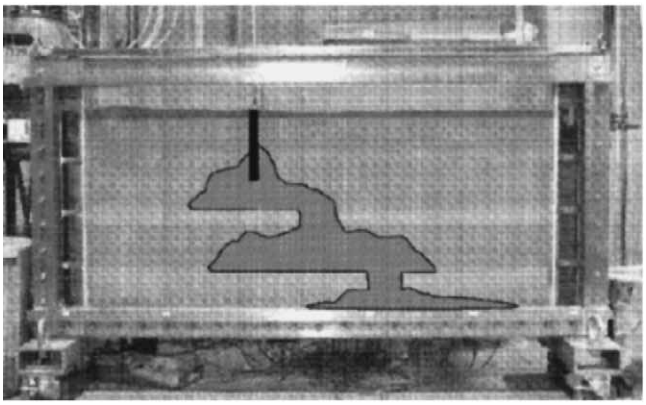

(c)

Fig. 5. HFE migration results with lateral groundwater flow, $i = 0.033$: (a) 1 h after; (b) 4 h after; and (c) 7 h after. Pore water was introduced from left to right.

accumulates to a height of 24 cm on the quasi-aquitard, HFE will invade into the quasi-aquitard. However, even though the height of HFE on the lower quasi-aquitard exceeded 24 cm, no infiltration of HFE into the quasi-aquitard was observed because the domain in which HFE can migrate exists in two dimensions in this tank test. As a result, the HFE that reaches the quasi-aquitard accumulates on the quasi-aquitard, but the pressure head of HFE is not directly applied to the top surface of the quasi-aquitard. Thus, HFE migrates in a horizontal domain where the required pressure head for HFE migration is lower than the displacement pressure head of the quasi-aquitard.

## 4. Computational results

In order to confirm the reliability of the experimental results and verify the availability of numerical analysis (computation) as a method for predicting two-phase flow in porous media, numerical analyses were performed using the two-dimensional finite difference code NAPL:Simulator [32]. This numerical code is able to consider multiphase flow by a continuity equation and the VG model with the scaling coefficient (Eq. (5)). For the numerical analysis, only the lower elevation portion of the bottom of the trench box is considered as the analytical domain, as shown in Fig. 6. A total of 7,950 (53-nodes height × 150-nodes width) rectangular elements were generated by this numerical analysis). The bottom boundary of the tank was impermeable to the water phase. The water pressure heads of both (left and right) sides and the top were fixed according to the initial conditions, thereby allowing water flow through the boundaries. DNAPL was spilled into the soil medium at a constant pressure head of 15.2 cm $H_2O$, which is equivalent to the 10 cm height difference of DNAPL having a density 1.52 g/cm$^3$. All boundaries of the tank were considered to be impermeable to the HFE phase except the spillage point. The properties of HFE tabulated in Table 3 were used in the numerical analysis as DNAPL; the density was 1.52 g/cm$^3$, the viscosity was $0.58 \times 10^{-3}$ Pa × *s*, and the interfacial tension was 35.59 mN/m. The properties of Toyoura and silica #7 sands summarized in Tables 1 and 2 were used in the numerical analysis so that the experimental and computational conditions would be the same; i.e. soil particle densities of Toyoura and silica #7 sands were 2.641 and 2.626 g/cm$^3$, hydraulic conductivities were $1.45 \times 10^{-2}$ and $2.33 \times 10^{-3}$ cm/s, dry (bulk) densities were 1.63 and 1.53 g/cm$^3$, residual water saturations were 0.14 and 0.20, and VG-parameters $\alpha_{AW}$ and $n$ were 0.0212 and 0.0102 cm$^{-1}$, and 6.57 and 5.70, respectively. For the condition without lateral groundwater flow, the two side boundaries were fixed at 0 cm $H_2O$ pressure head, i.e., no external pressure head was applied. By contrast, under the condition with lateral groundwater flow, the left-hand side boundary for the water phase was fixed at 5 cm $H_2O$ pressure head as an external pressure head in accordance with the experimental boundary conditions.

The computational results at 1, 4, and 7 h without lateral groundwater flow are shown in Fig. 7 with respect to the degree of DNAPL saturation. Fig. 7a shows that DNAPL was infiltrated from the spillage point, reached the upper quasi-aquitard, and migrated laterally along the top surface of the quasi-aquitard. The maximum degree of DNAPL saturation above the upper quasi-aquitard was approximately

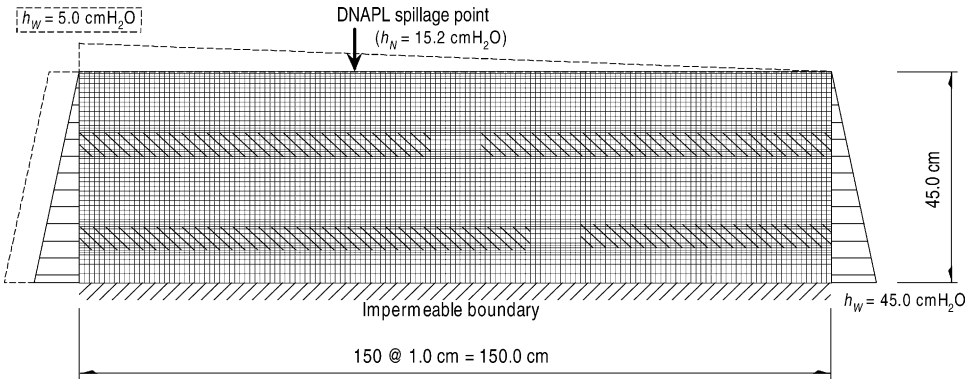


Fig. 6. Generated grid and boundary conditions for numerical analysis. The broken line is for the case with lateral groundwater flow from left to right. The downward diagonal hatch represents quasi-aquitard.

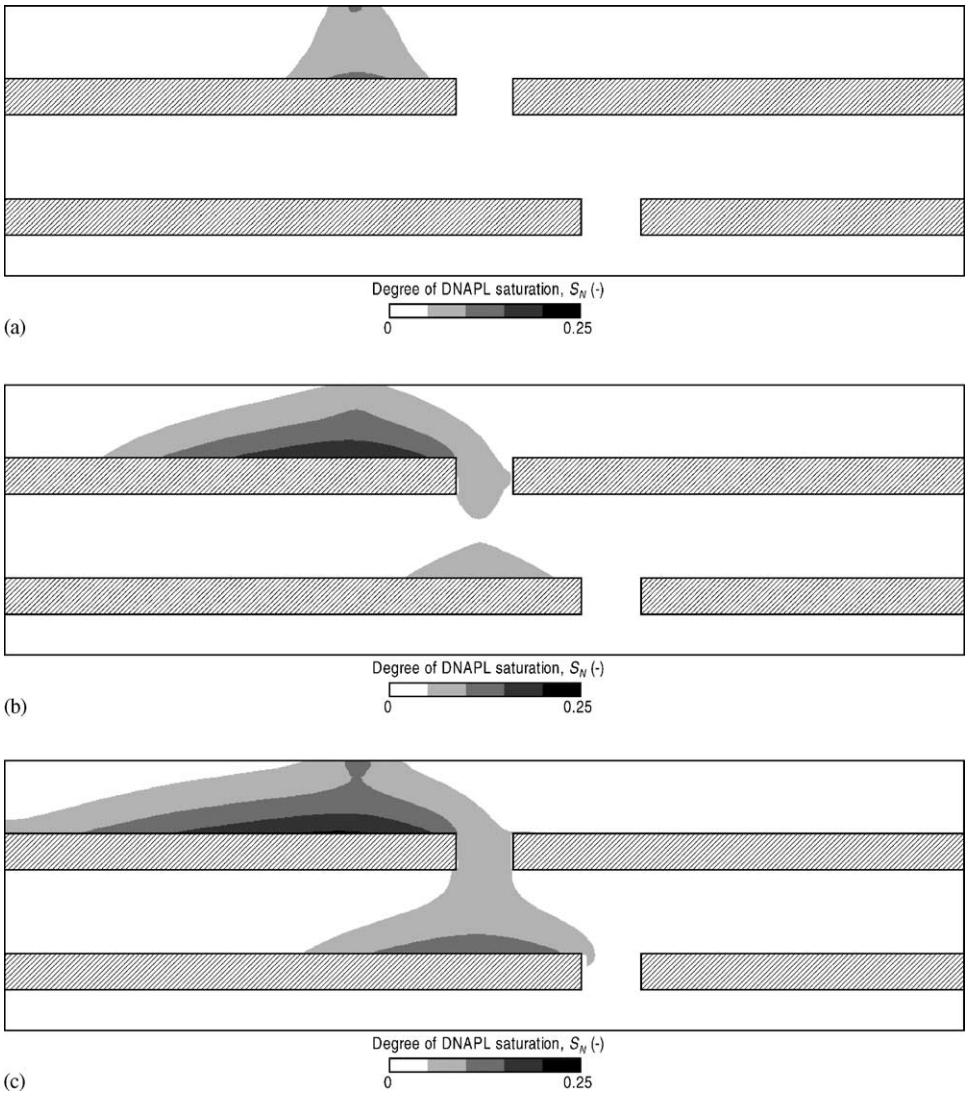


Fig. 7. Computational results without lateral groundwater flow, $i = 0.000$: (a) 1 h after; (b) 4 h after; and (c) 7 h after.

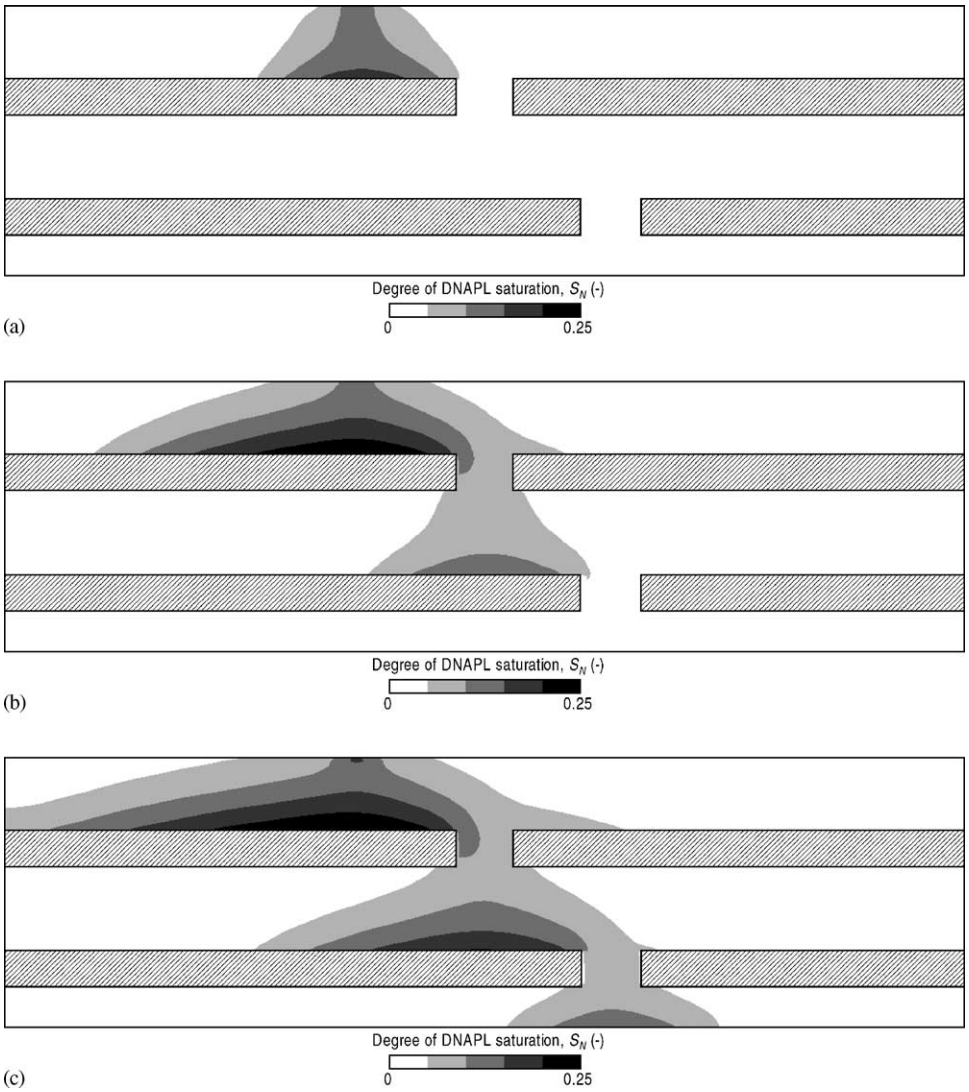


Fig. 8. Computational results WITH lateral groundwater flow, $i = 0.000$: (a) 1 h after; (b) 4 h after; and (c) 7 h after.

0.1. The discontinuous contour point seen at the center in Fig. 7b was due to the fact that the degree of DNAPL saturation at that point was less than 0.05; nevertheless, DNAPL did exist. The DNAPL that migrated laterally did not reach the right, upper quasi-aquitard, and all DNAPL penetrated the crack.

Fig. 8 shows the computational results at 1, 4, and 7 h with lateral groundwater flow. The DNAPL in Fig. 8a was more widely spread than that in Fig. 7a without groundwater flow. In contrast with the computational results for the case without groundwater flow, DNAPL migration with lateral groundwater flow was observed at the right-hand side of the upper quasi-aquitard, and DNAPL reached the bottom of the tank after 7 h, as shown in Fig. 8c. From the results of the numerical analysis (computation), lateral groundwater flow with a hydraulic gradient of 0.033 can transport DNAPL sideward, and DNAPL with lateral groundwater flow migrates faster than that without groundwater flow.

## 5. Discussion

To compare experimental and computational results, the results obtained after 10 h are discussed herein. The experimental and computational results without or with lateral groundwater flow are shown in Figs. 9 and 10, respectively. To clearly visualize the DNAPL distribution, the outlines were retouched by hand tracing (dashed line in Fig. 9). Although an additional 3 h had passed as compared with the photographs shown in Figs. 4c and 5c, little change in the DNAPL distribution was seen except at the tank bottom (Fig. 9). For the case with lateral groundwater flow, it was observed that DNAPL did not reach the right upper quasi-aquitard even at 10 h.

Fig. 10 shows the computational results without or with lateral groundwater flow with respect to the degree of DNAPL saturation (five-step contours in this figure) and the DNAPL flow direction that expresses the difference in

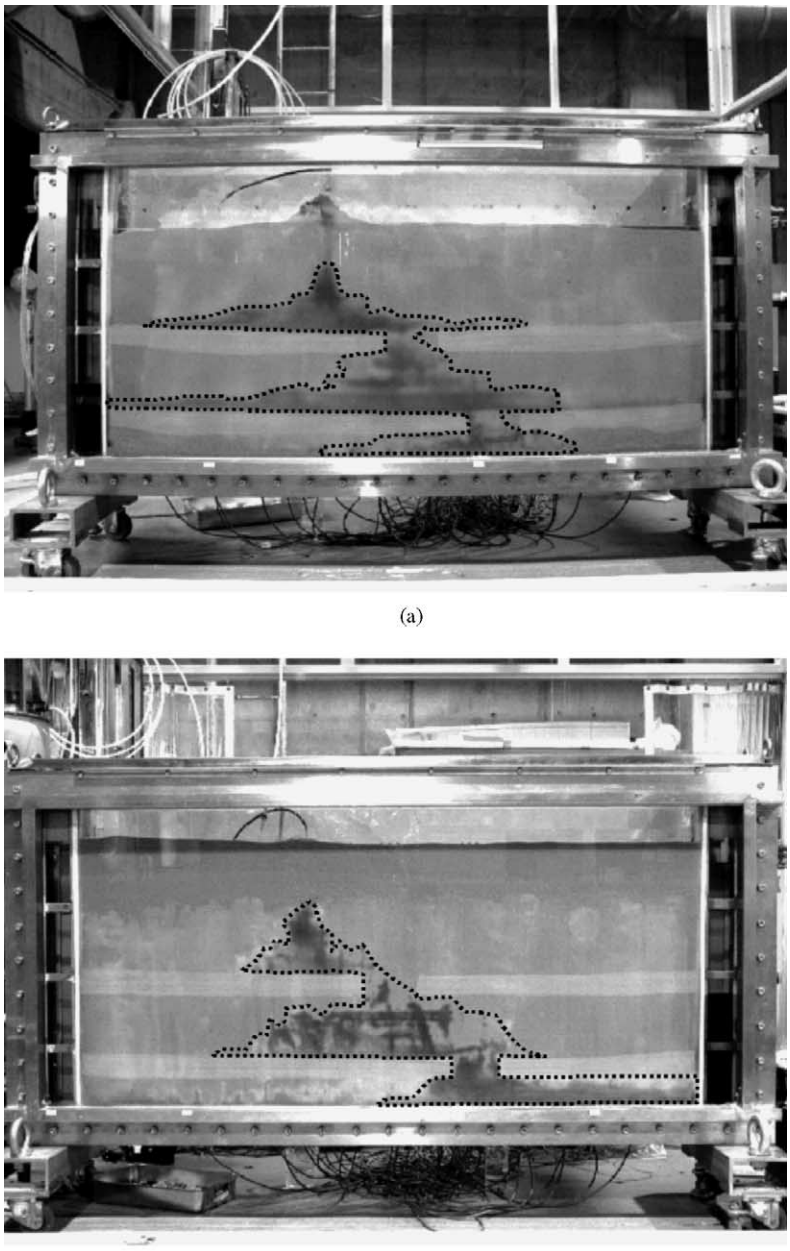

(a)

(b)

Fig. 9. DNAPL distribution after 10 h: (a) without lateral groundwater flow and (b) with lateral groundwater flow.

relative velocity (white arrowheads). Two significant points are apparent: (1) the migration rate of DNAPL with lateral groundwater flow (Fig. 10b) is higher than that without groundwater flow (Fig. 10a), as evident by a significant difference in the flow rate of DNAPL is seen at the cracks of the quasi-aquitards, and (2) DNAPL migrates more widely to both sides with lateral groundwater flow than without groundwater flow.

From comparison of the experimental and computational results without groundwater flow (Figs. 9a and 10a, respectively), revealed that DNAPL in the experiment reached the right upper quasi-aquitard, whereas the DNAPL in the numerical analysis did not. In contrast, for the results with lateral groundwater flow shown in Figs. 9b and 10b, lateral DNAPL migration to the right upper quasi-aquitard was found in the computational result but not in the experiment. Hence, the standard multiphase flow model that uses both the continuous equation for flow phases and the element method was not able to simulate all the realistic phenomena occurring in immiscible two-phase flow with lateral groundwater flow. In addition, a notable observation is that the DNAPL reached the right-hand sides of both upper and lower quasi-aquitards in the experimental results without groundwater flow, whereas it reached only the right lower quasi-aquitard unlike the upper quasi-aquitard in the case with lateral groundwater flow.

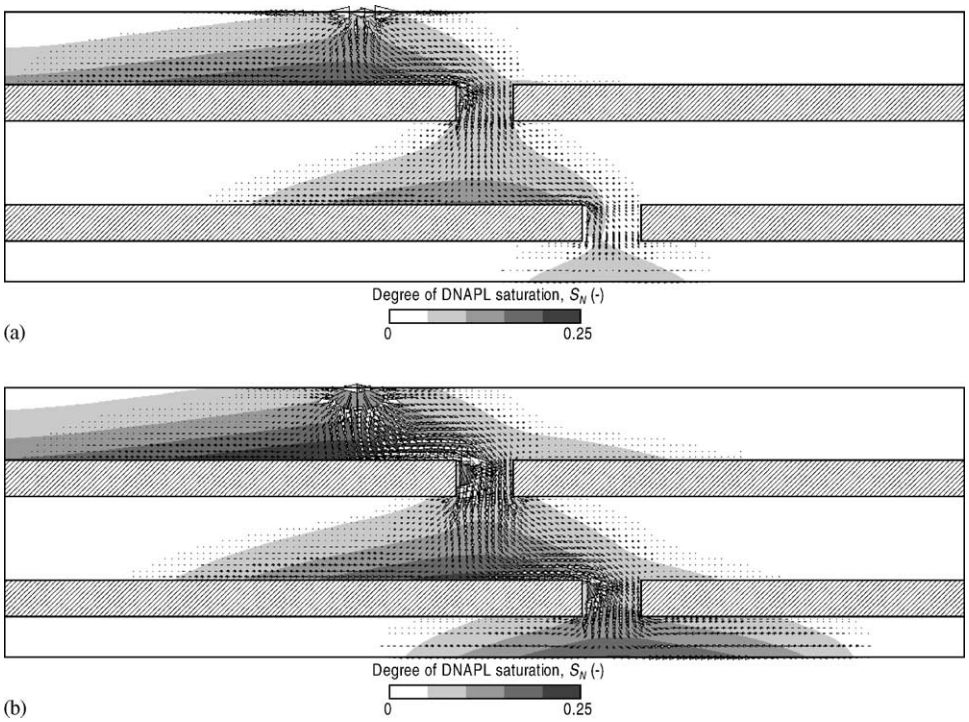


Fig. 10. Computational results for degree of DNAPL saturation (contour) and DNAPL flow direction (arrow) after 10 h: (a) without lateral groundwater flow and (b) with lateral groundwater flow.

The difference in the DNAPL migration rate at the mouth of the crack in the quasi-aquitard is considered to be one of the reasons for the difference in lateral DNAPL migration at the crack. It is observed from the computational results in Fig. 10 that the migration rate of DNAPL at the upper crack is higher than that at the lower crack, and the migration rate with lateral groundwater flow is higher than that without groundwater flow. Assuming that the flow rate distribution in the computational results is consistent with that in the experimental results, the following two points can be inferred: (i) in the water–DNAPL two-phase system, DNAPL migrates bilaterally under relatively low lateral groundwater flow rates or no flow condition, even though there is the crack in an aquitard; and (ii) DNAPL migrates preferentially to the bottom when there is a relatively high lateral flow rate of groundwater. In other words, lateral groundwater flow promotes the downward migration of DNAPL.

The difference in transitional domain between DNAPL and water is also significant. For example, the computational results revealed a large transitional domain between DNAPL and water, which is indicated by the gentle gradient in the degree of saturation, whereas the transitional domain between the two fluids in the experiment is very small (Fig. 11). Although the element (grid) method is one of the methods used for numerical approximation, it is unsuitable for calculating rapid variations, and the slope of the transitional domain depends on the grid space. Thus, a gentle gradient results from the computational analysis. It is inferred that under actual conditions, DNAPL migrates sharply in the pore space in the form of a step function.

The computational results of pore DNAPL pressure at points B and C in Fig. 3 were compared with experimental results obtained by measurements with hydrophobic tensiometers. No change in pore water pressure as measured by hydrophilic tensiometers was observed in the experiments. The results obtained without and with lateral groundwater flow are shown in Fig. 12a and b, respectively. In the case without lateral groundwater flow, the experimental results

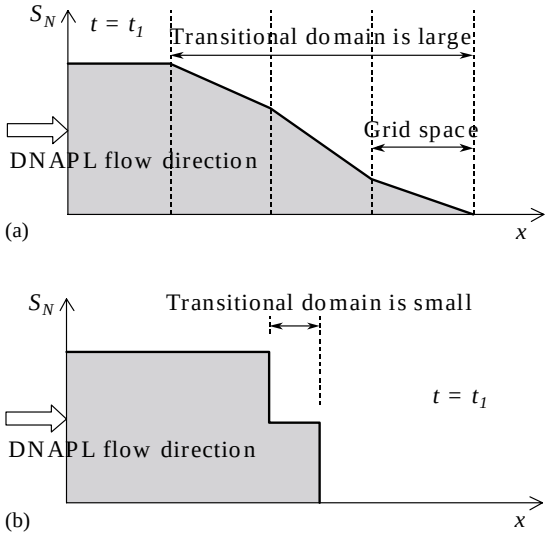


Fig. 11. Difference between computational result and actual degree of DNAPL saturation, $S_N$, $t = t_1$: (a) computational result and (b) actual distribution of the degree of DNAPL saturation.

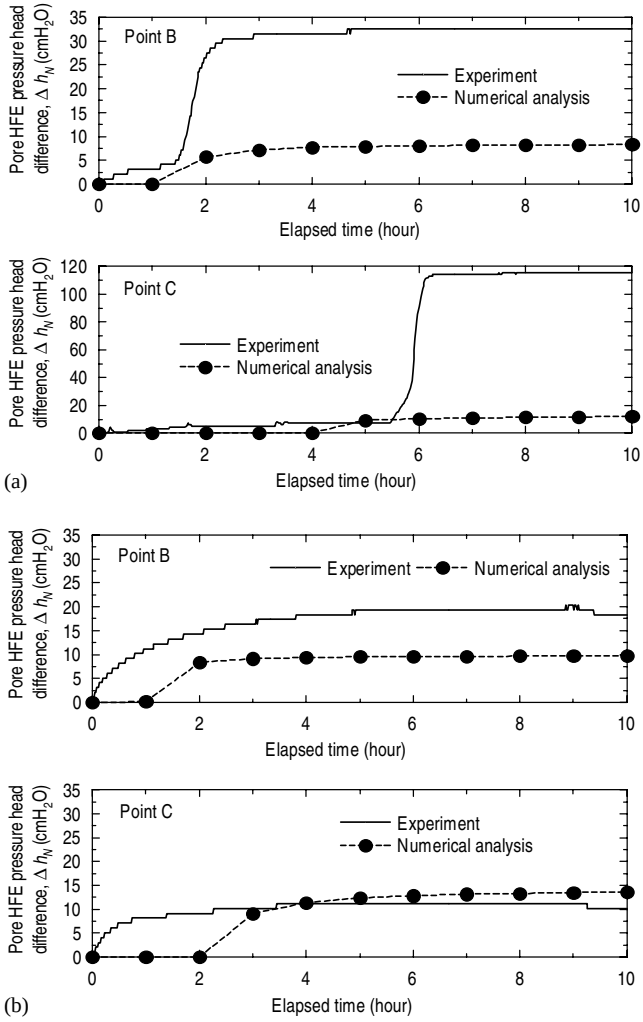


Fig. 12. Pore HFE pressure head profiles at points B and C: (a) without lateral groundwater flow and (b) with lateral groundwater flow. $h$ is defined as the difference between initial and measuring pore DNAPL pressure.

exceeded the computational results at both points B and C, and the difference was marked at point C. This is probably because the difference depends on whether or not excess pore DNAPL pressure disperses. In the absence of groundwater flow, there is no migration of pore water, and hence DNAPL can migrate only by displacing the water from the pore space. Consequently, a large pore DNAPL pressure is required for migration, and the excess pore DNAPL pressure is not immediately dispersed. In computing multiphase flow, pore-water and DNAPL pressures are treated as independent parameters, and those pressures are controlled by the *S–p* relation. Thus, simulating the mechanism involved in displacing water from the pore space by DNAPL and DNAPL migrating with pore water at the same time may be difficult. In the case with lateral groundwater flow shown in Fig. 12b, the pore DNAPL pressure obtained in the experimental result is higher than or equal to that obtained by numerical analysis. The reason for this difference may be that DNAPL migrates to disperse immediately excess pore DNAPL pressure, because the rate of the lateral groundwater flow is relatively high.

The difference in the increase in the pore DNAPL pressure in the experimental results is also notable. In contrast to the steeply increasing pore DNAPL pressure in the case without groundwater flow, the pore DNAPL pressure gradually increases in the case with lateral groundwater flow. The pore pressure difference between experimental and computational results and the preferential downward flow of DNAPL (mentioned above) are considered to be due to the difference between the static and dynamic interfacial tensions in the water–DNAPL two-phase system. Although the static interfacial tension is used in the calculation of the scaling coefficient and the *S–p* relation is generally depicted under static conditions, dynamic interfacial tension would be required for estimating DNAPL migration with higher accuracy.

## 6. Conclusions

This paper describes the influence of lateral groundwater flow on DNAPL migration in an unconfined aquifer. The main results obtained from both experiment and numerical analysis are as follows:

1. The laboratory-scale tank test enabled successful visualization of DNAPL migration with or without lateral groundwater flow. The effects of lateral groundwater flow on two-dimensional DNAPL migration were observed.
2. No DNAPL infiltration into the quasi-aquitard having a relatively high displacement pressure head was observed. In this study, the quasi-aquitard consisted of silica #7 sand with $k = 2.3 \times 10^{-3}$ cm/s of $e = 0.72$.
3. In the case without groundwater flow, DNAPL showed preference for bilateral migration (right and left symmetry) rather than vertical migration to the bottom, and an elliptical spread from the spillage point was observed.
4. For the case with lateral groundwater flow, lateral DNAPL migration was not affected by the lateral groundwater flow.
5. Experiments revealed that lateral groundwater flow with a hydraulic gradient of 0.033 did not transport DNAPL in the lateral direction in an unconfined aquifer having a hydraulic conductivity of $10^{-2}$ cm/s; rather, it promoted the downward migration of DNAPL.
6. The results of the numerical analysis roughly approximated the observed two-dimensional DNAPL migration; however, the numerical analysis was not able to accurately mimic the observed step-function-like migration. Thus, the expression of DNAPL migration by both the governing equation and the element (grid) method may have certain limitations.
7. The hydrophobic tensiometer was able to detect the pore DNAPL pressure in the two-dimensional tank test; however, not all the measured pressures were consistent with the computational results.

The effect of lateral groundwater flow on two-dimensional DNAPL migration in an unconfined aquifer was experimentally clarified. As the rate of lateral groundwater flow is increased by pumping for contaminated groundwater remediation, there is a possibility of inducing an unexpected downward migration of DNAPL.

## Acknowledgements

The laboratory-scale tank test was conducted at Kajima Technical Research Institute (KaTRI). The support provided by Dr. Hiroshi Abe of KaTRI is greatly acknowledged. The technical contributions and comments of Mr. Keijirou Ito and Mr. Keisaku Yasumoto of KaTRI are highly appreciated.

## References

[1] I. Chatzis, F.A.L. Dullien, Dynamic immiscible displacement mechanisms in pore doublets: theory versus experiment, J. Colloid Interface Sci. 91 (1) (1983) 199–222.
[2] D.F. Lowe, C.L. Oubre, C.H. Ward (Eds.), Surfactants and Cosolvents for NAPL Remediation: A Technology Practices Manual, CRC Press, 1999.
[3] P.J. Hensley, A.N. Schofield, Accelerated physical modelling of hazardous-waste transport, Géotechnique 41 (3) (1991) 447–465.
[4] R.K. Rowe, T.R. Weaver, Contaminant transport in groundwater, in: A. Bouazza, J. Kodikara, R. Parker (Eds.), GeoEnvironment97, Balkema, 1997, pp. 97–13.
[5] M.H. Roper, A.O. Thomas, S. Jefferis, G.H. Norris, The reactive barrier—a novel use of scrap iron to clean up chlorinated solvent contaminated groundwater, in: R.N. Yong, H.R. Thomas (Eds.), Geoenvironmental Engineering, Thomas Telford, London, 1997, pp. 484–489.
[6] M. Shimomura, S. Imamura, T. Nagatou, T. Motoyama, Transport and biodegradation phenomena of volatile chlorinated hydrocarbon, in: M. Kamon (Ed.), Environmental Geotechnics, Balkema, Rotterdam, 1996, pp. 1079–1082.
[7] M. Vogler, U. Arslan, R. Katzenbach, The influence of capillarity on multiphase flow within porous media—a new model for interpreting fluid levels in groundwater monitoring wells in dynamic aquifers, in: R.N. Yong, H.R. Thomas (Eds.), Geoenvironmental Engineering, Thomas Telford, London, 1999, pp. 318–325.
[8] D.G. Grubb, L.E. Empie, G.W. Hudock, R.N. Davis, S.B. Lathrop, Mobilization of toluene in layered, unconfined aquifer media during ethanol flooding, in: Sêco e Pinto (Ed.), Environmental Geotechnics, 1998, pp. 449–454.
[9] G.S. Walser, T.H. Illangasekare, A.T. Corey, Retention of liquid contaminants in layered soils, J. Contam. Hydrol. 39 (1999) 91–108.
[10] T.C. Neumann, A.J. Valsangkar, K.T. MacQuarrie, Physical modeling of LNAPL infiltration in a variably-saturated sand, GeoEng2000 On CD-ROM.
[11] L.J.J. Catalan, F.A.L. Dullien, Application of gravity drainage to the recovery of residual LNAPL in homogeneous and lensed sand packs, J. Contam. Hydrol. 18 (1995) 279–306.
[12] M. Oostrom, R.J. Lenhard, Comparison of relative permeability-saturation-pressure parametric models for infiltration and redistribution of a light nonaqueous-phase liquid in sandy porous media, Adv. Water Res. 21 (2) (1998) 145–157.
[13] M. Kamon, K. Endo, T. Katsumi, Experimental investigation on the properties of DNAPLs migration, in: R.N. Yong, H.R. Thomas (Eds.), Geoenvironmental Engineering, Thomas Telford, London, 2001, pp. 307–312.
[14] C. Hofstee, R.C. Walker, J.H. Dane, Infiltration and redistribution of perchloroethylene in stratified water-saturated porous media, Soil Sci. Soc. Am. J. 62 (1998) 13–22.
[15] M. Oostrom, C. Hofstee, R.C. Walker, J.H. Dane, Movement and remediation of trichloroethylene in a saturated heterogeneous porous medium, 1. spill behavior and initial dissolution, J. Contam. Hydrol. 37 (1999) 159–178.
[16] C. Hofstee, M. Oostrom, J.H. Dane, R.C. Walker, Infiltration and redistribution of perchloroethylene in partially saturated, stratified porous media, J. Contam. Hydrol. 34 (1998) 293–313.
[17] G.M. Shook, G.A. Pope, K. Kostarelos, Prediction and minimization of vertical migration of DNAPLs using surfactant enhanced aquifer remediation at neutral buoyancy, J. Contam. Hydrol. 34 (1998) 363–382.
[18] K. Kostarelos, G.A. Pope, B.A.R.G.M. Shook, A new concept: the use of neutrally-buoyant microemulsions for DNAPL remediation, J. Contam. Hydrol. 34 (1998) 383–397.
[19] M. Oostrom, C. Hofstee, R.C. Walker, J.H. Dane, Movement and remediation of trichloroethylene in a saturated, heterogeneous porous medium, 2. pump-and-treat and surfactant flushing, J. Contam. Hydrol. 37 (1999) 179–197.
[20] P.K. Padgett, N.J. Hayden, Mobilization of residual tetrachloroethylene during alcohol flushing of clay-containing porous media, J. Contam. Hydrol. 40 (1999) 285–296.
[21] K.D. Pennel, G.A. Pope, L.M. Abriola, Influence of viscous and buoyancy forces on the mobilization of residual tetrachloroethylene during surfactant flushing, Environ. Sci. Technol. 30 (4) (1996) 1328–1335.
[22] C.B. Andrews, The great American experiment: pump-and-treat for groundwater cleanup, in: Proceedings of the International Symposium on Groundwater Contamination (ISGC), 2000, pp. 1–8.
[23] E.A. Voudrias, Pump-and-treat remediation of groundwater contaminated by hazardous waste: can it really be achieved? Int. J. Global Nest 3 (1) (2001) 1–10.
[24] M.T. van Genuchten, A closed-form equation for predicting the hydraulic conductivity of unsaturated soils, Soil Sci. Soc. Am. J. 44 (1980) 892–898.
[25] R.H. Brooks, A.T. Corey, Hydraulic properties of porous media, in: Hydrology Paper no.3, Colorado State University, Fort Collins, 1964, pp. 1–27.
[26] Y. Mualem, A new model for predicting the hydraulic conductivity of unsaturated porous media, Water Resour. Res. 12 (3) (1976) 513–522.
[27] C. Huh, S.G. Mason, A rigorous theory of ring tensiometry, Colloid Polym. Sci. 253 (1975) 566–580.
[28] A.K. Katyal, J.J. Kaluarachchi, J.C. Parker, MOFAT: a two-dimensional finite element program for multiphase flow and multicomponent transport, EPA/600/2-91/020, U.S.EPA, 1991.
[29] R.J. Lenhard, J.C. Parker, Measurement and prediction of saturation-pressure relationships in three-phase porous media systems, J. Contam. Hydrol. 1 (1987) 407–424.
[30] J.C. Parker, Multiphase flow and transport in porous media, Rev. Geophys. 27 (3) (1989) 311–328.
[31] Z.S. Abu-Hassanein, M.Pantazidou, M.F. Riemer, Infiltration of high viscosity low density DNAPLs in saturated porous media, in: T. Kimura, O. Kusakabe, J. Takemura (Eds.), Centrifuge 98, Balkema, Rotterdam, 1998, pp. 595–599.
[32] J. Guarnaccia, G. Pinder, M. Fishman, NAPL: simulator documentation, EPA/600/R-97/102, U.S.EPA, 1998.